J Nanostruct 16(4): 4728-4743, Autumn 2026

RESEARCH PAPER

Study the Effect of Zinc oxide Nanoparticles on the Liver Tissue Morphometric Analysis of Newborn Mice After Inoculation During Pregnancy

Russul Kareem Nasir [1], ***Mazin Kamil Hamid*** [1]*, ***Haider Abdulrasool Jaafar*** [2]

[1] *Department of Physiology and Medical Physics, College of Medicine, Al-Nahrain University, Baghdad, Iraq*

[2] *Department of Anatomy, College of Medicine, Al-Nahrain University, Baghdad, Iraq*

ARTICLE INFO

Article History:
Received 17 May 2026
Accepted 11 July 2026
Published 01 October 2026

Keywords:
Hematoxylin
Hepatotoxicity
Immunohistochemistry
Neonatal liver
Tumor necrosis factor

ABSTRACT

Zinc oxide nanoparticles (ZnO NPs) have attracted considerable attention owing to their unique properties and broad biomedical applications. Their hepatic safety profile during prenatal development remains incompletely understood. This study aimed to synthesize ZnO NPs by chemical precipitation and evaluate their dose-dependent effects on the liver of newborn mice following maternal intraperitoneal exposure. ZnO NPs were synthesized by chemical precipitation and characterized by FESEM, XRD, UV-visible spectrophotometry, and zeta potential analysis. Forty adult Swiss albino female mice (20–25 g) were allocated into five equal groups. Group A (control) received intraperitoneal distilled water daily for 18 days. Groups B–E received ZnO NPs at 5, 10, 20, and 30 mg/kg daily for 18 days. Neonatal liver specimens were fixed in formalin, paraffin-embedded, sectioned at 5 µm, and stained with hematoxylin and eosin for histological evaluation. ZnO NPs showed a mean particle size of 20–25 nm with crystalline hexagonal wurtzite structure confirmed by XRD. Histological examination revealed progressive, dose-dependent hepatocellular injury characterized by hepatic plate thinning, vacuolation, pyknotic nuclei, ghost cells, and extensive necrosis, most pronounced at higher doses. Congested vessels with inflammatory infiltration and red blood cell invasion into the parenchyma were prominent in high-dose groups. Morphometric analysis revealed significant reduction in hepatic plate thickness across groups ($p = 0.0001$). Maternal ZnO NP exposure induces significant, dose-dependent hepatotoxicity in neonatal mouse liver, evidenced by progressive histological deterioration and morphometric shrinkage of hepatic plates, underscoring the need for rigorous prenatal safety evaluation of these nanomaterials.

How to cite this article
Nasir R, Hamid M, Jaafar H. Study the Effect of Zinc oxide Nanoparticles on the Liver Tissue Morphometric Analysis of Newborn Mice After Inoculation During Pregnancy . J Nanostruct, 2026; 16(4):4728-4743. DOI: 10.22052/JNS.2026.04.022

INTRODUCTION

The past two decades have witnessed a remarkable expansion in the application of nanotechnology to the biomedical sciences. Nanoparticles — defined as particles with at least one dimension in the range of 1-100 nm exhibit physicochemical properties that differ fundamentally from their bulk counterparts,

* *Corresponding Author Email: mazinkamil4@gmail.com*

including dramatically increased surface-area-to-volume ratios, quantum confinement effects, and enhanced chemical reactivity [1]. These unique characteristics have positioned metal oxide nanoparticles at the forefront of biomedical research, where they are being actively investigated for applications ranging from drug delivery and cancer theranostics to antimicrobial coatings and diagnostic imaging [2].Among the metal oxide nanoparticles that have received the most intensive scientific scrutiny, zinc oxide nanoparticles (ZnO NPs) occupy a particularly prominent position. Zinc oxide nanoparticles have been proven to exhibit strong antimicrobial effects, and the U.S. Food and Drug Administration (FDA) considers ZnO as GRAS (generally recognized as safe) [3]. It has wide applications as a food additive, as excipients in pharmaceutical formulations, cosmetics, and implant materials [3]. In the biomedical domain, ZnO NPs have been explored for their potent antibacterial activity, antifungal properties, wound healing promotion, anticancer drug delivery, and bioimaging applications [4]. Their wide direct bandgap of approximately 3.37 eV and large exciton binding energy of 60 meV at room temperature confer exceptional optical properties including strong ultraviolet absorption and photoluminescence, characteristics that are exploited in both therapeutic and diagnostic applications [5].

A variety of physical, chemical, and biological methods have been developed for the synthesis of ZnO NPs, each offering distinct advantages and limitations with respect to particle size, morphology, crystallinity, purity, cost, and scalability [6]. The chemical precipitation method, employed in the present study, represents one of the simplest, most cost-effective, and most reproducible routes to the fabrication of ZnO NPs with well-controlled physicochemical characteristics. This approach involves the reaction of a zinc salt precursor with an alkaline precipitating agent to produce a zinc hydroxide intermediate, which is subsequently converted to crystalline ZnO through thermal annealing [7]. The method allows precise control of particle size and morphology through adjustment of reaction parameters including precursor concentration, pH, temperature, and annealing conditions, and produces nanoparticles with the high crystallinity essential for reproducible biological evaluation [7].

Despite the growing commercial and biomedical utilization of ZnO NPs, a substantial and expanding body of evidence has raised concerns regarding their potential toxicity in biological systems. The primary mechanisms by which ZnO NPs exert cellular toxicity include the dissolution of the nanoparticle core with release of cytotoxic zinc ions (Zn^{2+}) into the intracellular environment, the generation of reactive oxygen species (ROS) through both particle-mediated and ion-mediated pathways, and direct physical interaction of the nanoparticle surface with cellular membranes and organelles [8]. These mechanisms are interrelated and frequently operate simultaneously, producing a complex pattern of cellular injury that includes oxidative DNA damage, mitochondrial dysfunction, lysosomal destabilization, and activation of intrinsic apoptotic pathways [9]. The central role of the liver in detoxification, metabolism and excretion makes this vital organ a crucial target of ZnO NPs [10]. The liver is recognized as the primary organ of nanoparticle accumulation following systemic administration, owing to the fenestrated sinusoidal endothelium of the hepatic vasculature and the phagocytic activity of resident Kupffer cells [11]. As the central metabolic organ, the liver is therefore disproportionately exposed to circulating nanoparticles and their released ionic products, making hepatotoxicity one of the most clinically significant concerns associated with ZnO NP exposure. Multiple in vitro and in vivo studies have confirmed the hepatotoxic potential of ZnO NPs, with findings including hepatocyte degeneration, necrosis, sinusoidal congestion, and inflammatory cell infiltration [10, 12].

While the hepatotoxic effects of ZnO NPs in adult animals have been relatively well characterized, comparatively little attention has been directed toward the consequences of ZnO NP exposure during pregnancy and its effects on the developing fetal and neonatal liver. This is a critical knowledge gap, as nanoparticles administered to pregnant animals have been shown to cross the placental barrier and accumulate in fetal tissues, with the fetal liver representing a major site of nanoparticle deposition [13]. The fetal and neonatal liver is particularly vulnerable to toxic insults for several reasons: it serves as the primary site of hematopoiesis during the prenatal and early postnatal period, meaning that hepatic injury necessarily disrupts erythrocyte production; its detoxification enzyme systems, including cytochrome P450 isoforms, are immature

and therefore less capable of metabolizing or neutralizing toxic compounds; and its hepatocyte proliferation rates are substantially higher than in the adult liver, potentially amplifying the genotoxic consequences of nanoparticle-mediated DNA damage [14]. Maternal exposure to ZnO NPs during pregnancy therefore poses a dual risk: direct hepatotoxicity in the pregnant animal, and indirect developmental hepatotoxicity in the offspring through placental transfer and subsequent accumulation in the fetal and neonatal liver [15].

Given the rapidly expanding production and commercial use of ZnO NPs, and the critical knowledge gaps that persist regarding their safety during prenatal development, the present study was designed to provide a systematic, multi-parameter evaluation of the dose-dependent effects of maternally administered ZnO NPs on the liver of neonatal mice. Specifically, the study aimed to:

Synthesize and characterize ZnO NPs using the chemical precipitation method, confirming their physicochemical properties by TEM, XRD, UV–visible spectrophotometry, FESEM-EDS, and zeta potential analysis.

Evaluate the dose-dependent histological effects of maternal ZnO NP exposure on the hepatic architecture of neonatal mouse liver, including assessment of hepatic cell plate thickness, hepatocyte morphology, sinusoidal structure, and the nature and extent of hepatocellular injury.

Establish dose-response relationships for ZnO NP-mediated neonatal hepatotoxicity that may inform safety threshold determinations for maternal ZnO NP exposure.

MATERIALS AND METHODS

Ethical Approval

All experimental procedures involving animals were conducted in strict accordance with internationally recognized guidelines for the care and use of laboratory animals. The study protocol was reviewed and approved by the institutional animal ethics committee prior to the commencement of any experimental work. All efforts were made to minimize animal suffering and to reduce the number of animals used to the minimum required for statistically valid results.

Synthesis of Zinc Oxide Nanoparticles

ZnO NPs were synthesized by the chemical precipitation method, which was selected for its simplicity, reproducibility, cost-effectiveness, and capacity to yield phase-pure, crystalline nanoparticles of controlled dimensions under mild reaction conditions [6]. In brief, a precursor solution of zinc nitrate hexahydrate [$Zn(NO_3)_2 \cdot 6H_2O$] was prepared by dissolving an appropriate quantity of the salt in deionized water under continuous magnetic stirring at room temperature until complete dissolution was achieved. A sodium hydroxide (NaOH) solution of defined molarity was prepared separately in deionized water and added dropwise to the zinc nitrate solution under vigorous and continuous magnetic stirring. The dropwise addition of NaOH served as the alkaline precipitating agent, raising the pH of the reaction mixture and initiating the controlled nucleation and precipitation of zinc hydroxide [$Zn(OH)_2$] according to the following reaction:

$$Zn(NO_3)_2 + 2NaOH \rightarrow Zn(OH)_2\downarrow + 2NaNO_3$$

The reaction mixture was maintained under continuous magnetic stirring at a controlled temperature of 75°C for 30 minutes, allowing the precipitation reaction to proceed to completion and ensuring homogeneous particle nucleation throughout the reaction volume. Following the completion of the reaction period, the mixture was removed from the magnetic stirrer and allowed to settle. In order to eliminate residual ionic impurities including unreacted zinc nitrate, sodium nitrate by-product, and excess sodium hydroxide the resulting precipitate was subjected to three successive cycles of washing with deionized water, with careful decantation or vacuum filtration between each washing cycle. The washed white precipitate was collected and transferred to ceramic crucibles, then subjected to a two-stage thermal treatment in a programmable electrical furnace:

Stage 1 - Drying: The precipitate was dried at 100°C for 3 hours to remove residual surface moisture and to complete the dehydration of any remaining $Zn(OH)_2$ intermediate.

Stage 2 - Calcination**:** A portion of the dried material was subsequently calcined at 500°C for 3 hours to promote complete thermal decomposition of the zinc hydroxide intermediate, full crystallization of the hexagonal wurtzite ZnO phase, and elimination of any residual contaminants:

$Zn(OH)_2 \rightarrow ZnO + H_2O$

The calcined white powder was allowed to cool to room temperature in a desiccator and was then stored in sealed glass vials under dry, light-protected conditions until use. Fig. 1 provides a schematic illustration of the complete synthesis and purification workflow.

Physicochemical Characterization of ZnO NPs

The crystalline phase and purity of the synthesized ZnO NPs were determined by powder X-ray diffraction (XRD) using a diffractometer equipped with Cu Kα radiation (λ = 0.15406 nm) over a 2θ scanning range of 20°–80°. Diffraction peaks were indexed by comparison with the standard reference pattern for hexagonal wurtzite ZnO (JCPDS card No. 36-1451). The mean crystallite size was calculated from the most intense diffraction peak using the Scherrer equation:

$$D = K\lambda / \beta \cos\theta$$

where D is the mean crystallite diameter, K is the Scherrer constant (0.94 for spherical crystallites), λ is the X-ray wavelength (0.15406 nm), β is the full width at half maximum (FWHM) in radians, and θ is the Bragg diffraction angle.

UV–Visible Spectrophotometry

The optical absorption properties of the ZnO NPs were assessed by UV-visible spectrophotometry over the wavelength range of 200–800 nm. Nanoparticles were dispersed in deionized water at a defined concentration, and the absorption spectrum was recorded against a deionized water blank.

Field Emission Scanning Electron Microscopy with Energy Dispersive X-ray

The surface morphology and elemental composition of the synthesized ZnO NPs were examined using field emission scanning electron microscopy coupled with energy dispersive X-ray spectrometry. EDS spectra were acquired across an energy range of 0-10 keV to confirm elemental identity and chemical purity of the synthesized product.

Zeta Potential Analysis

The surface charge and colloidal stability of the ZnO NP suspension were evaluated by measuring the zeta potential analyzer. Measurements were performed in triplicate on freshly prepared aqueous suspensions of ZnO NPs at room temperature.

Preparation of ZnO NP Suspensions for Injection

Prior to each injection session, ZnO NPs were accurately weighed and suspended in sterile distilled water at the required concentrations (5, 10, 20, and 30 mg/kg body weight) by probe ultrasonication for 10 minutes to achieve a homogeneous and well-dispersed suspension. Freshly prepared suspensions were used for each day's injection to minimize the effects of particle sedimentation and aggregation over time. The injection volume was standardized to 0.1 mL per 10 g body weight for all groups.

Experimental Animals and Study Design

Forty adult Swiss albino female mice with body weights ranging from 20 to 25 g were obtained from a certified animal breeding facility. All animals were housed under standard laboratory conditions with a 12-hour light/dark cycle, controlled temperature (22 ± 2°C), and relative humidity of 50 ± 5%. Animals were provided with standard rodent chow and fresh tap water ad libitum throughout the experimental period, and were acclimatized to the laboratory environment for one week prior to the commencement of experimental procedures. All female mice were

Table 1. Experimental groups and ZnO nanoparticle treatment doses in pregnant Swiss albino mice.

Group	Designation	Treatment	Route	Duration
A	Control	Sterile distilled water	Intraperitoneal	Once daily, 18 days
B	Z0 — 5 mg/kg	ZnO NPs, 5 mg/kg body weight	Intraperitoneal	Once daily, 18 days
C	Z1 — 10 mg/kg	ZnO NPs, 10 mg/kg body weight	Intraperitoneal	Once daily, 18 days
D	Z2 — 20 mg/kg	ZnO NPs, 20 mg/kg body weight	Intraperitoneal	Once daily, 18 days
E	Z3 — 30 mg/kg	ZnO NPs, 30 mg/kg body weight	Intraperitoneal	Once daily, 18 days

mated with males of the same strain. Confirmation of pregnancy was established by observation of a vaginal plug (designated as gestational day 0) and by progressive monitoring of body weight gain over the subsequent days. Pregnant female mice were randomly allocated into five experimental groups of eight animals each, as Table 1.

Intraperitoneal injections were administered using a 26-gauge needle with care taken to avoid organ puncture. The injection site was rotated between the left and right lower abdominal quadrants on successive days to minimize local tissue irritation. All animals were monitored daily for clinical signs of toxicity including changes in body weight, coat condition, behavioral abnormalities, and mortality throughout the 18-day treatment period.

Tissue Collection and Histological Processing

Following completion of the 18-day treatment period and delivery of the offspring, neonatal mice pups were humanely euthanized and their liver specimens were immediately harvested under sterile conditions. Liver tissue samples were carefully dissected, rinsed briefly in ice-cold phosphate-buffered saline (PBS) to remove surface blood, and fixed by immersion in 10% neutral buffered formalin for a minimum of 24 hours at room temperature to ensure adequate tissue fixation and morphological preservation. Fixed tissue specimens were subsequently processed through a standard automated tissue processing protocol involving graded dehydration in ascending concentrations of ethanol (70%, 80%, 90%, 95%, and 100%), clearing in xylene, and impregnation and embedding in molten paraffin wax to produce paraffin tissue blocks. Serial sections of 5 µm thickness were cut from each paraffin block using a rotary microtome, mounted on glass slides, deparaffinized in xylene, and rehydrated through descending grades of ethanol to distilled water in preparation for staining.

Hematoxylin and Eosin Staining and Histomorphometric Analysis

For routine histological evaluation, deparaffinized and rehydrated tissue sections were stained with hematoxylin and eosin (H&E)

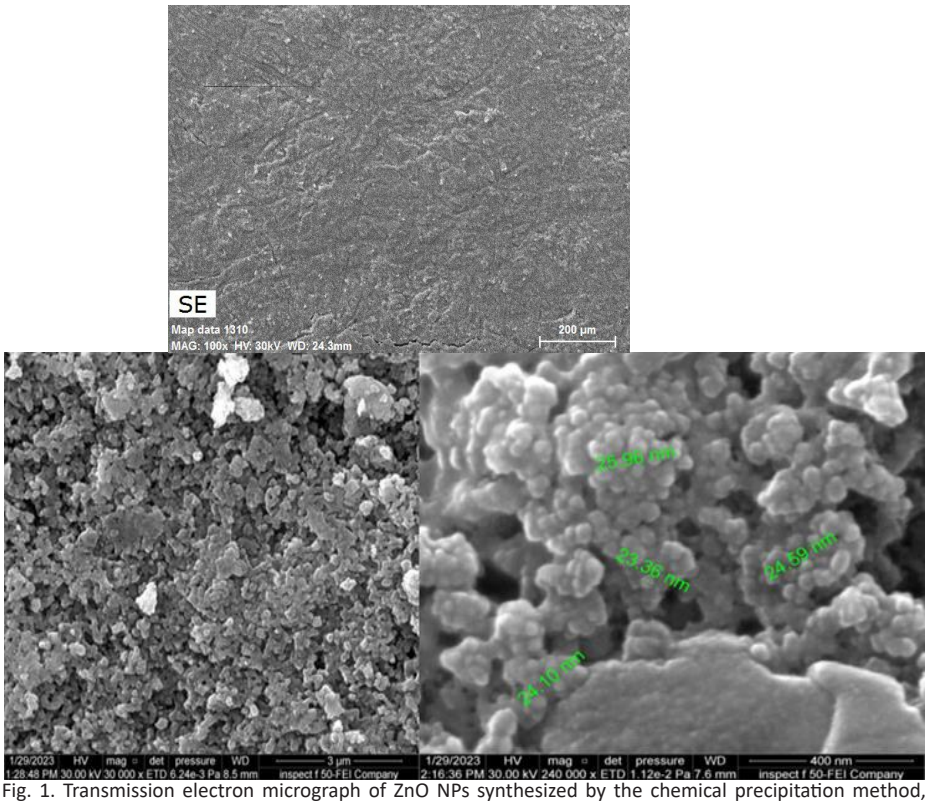

Fig. 1. Transmission electron micrograph of ZnO NPs synthesized by the chemical precipitation method, showing spherical morphology with a mean particle diameter of 20-25 nm.

according to the standard protocol. Sections were stained with Mayer's hematoxylin for 5 minutes, differentiated in 1% acid alcohol, blued in Scott's tap water substitute, counterstained with eosin Y for 2 minutes, dehydrated through ascending grades of ethanol, cleared in xylene, and coverslipped with DPX mountant. Histological assessment was performed by a blinded observer using a calibrated light microscope at magnifications of ×100 and ×400. The following histological parameters were systematically evaluated across all groups: hepatic cell plate and cord thickness; hepatocyte nuclear morphology (normal, pyknotic, karyolytic, or absent — ghost cells); cytoplasmic appearance (normal, vacuolated, or foamy); degree of sinusoidal congestion and red blood cell invasion; presence and distribution of inflammatory cell infiltrates (lymphocytes, monocytes, and macrophages); and extent of hepatic necrosis. For morphometric quantification, the thickness of hepatic cell plates and cords was measured in a minimum of ten randomly selected fields per section at ×400 magnification using calibrated digital image analysis. Results are expressed as mean ± standard deviation across all animals within each group.

Statistical Analysis

All quantitative data are expressed as mean ± standard deviation (SD). Statistical comparisons between experimental groups were performed using one-way analysis of variance (ANOVA) followed by appropriate post-hoc multiple comparison tests (Tukey's HSD or Bonferroni correction) using IBM SPSS Statistics software (version 26.0; IBM Corp., Armonk, NY, USA). A p-value of ≤ 0.05 was considered statistically significant, and a p-value of ≤ 0.001 was considered highly statistically significant.

RESULTS AND DICUSSION

Physicochemical Characterization of Synthesized ZnO NPs

Particle Size and Morphology

Field emission scanning electron microscopy (FESEM) analysis of the synthesized ZnO NPs as shown in Fig. 1 revealed a mean particle diameter in the range of 20–25 nm with a predominantly spherical morphology. The particles exhibited a narrow size distribution, indicative of the controlled nucleation and growth kinetics achieved under the optimized chemical precipitation conditions employed in this study.

UV–Visible Spectrophotometric Analysis

UV–visible spectrophotometric analysis of the synthesized ZnO NPs dispersed in deionized water was performed over the wavelength range of 200-1000 nm. As illustrated in Fig. 2, the absorption spectrum revealed a well-defined and sharp

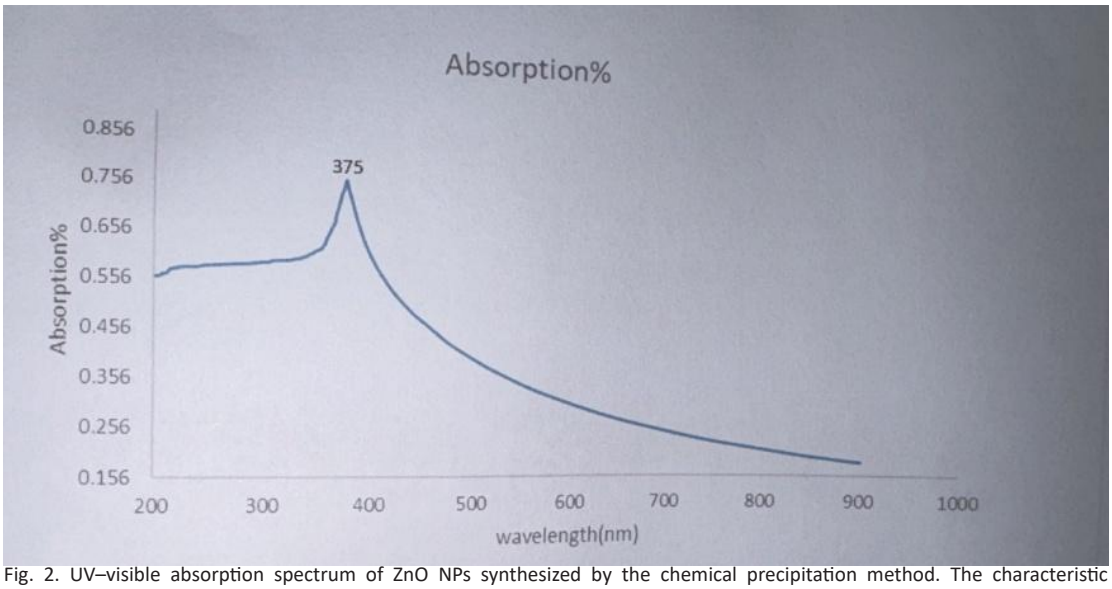

Fig. 2. UV–visible absorption spectrum of ZnO NPs synthesized by the chemical precipitation method. The characteristic absorption peak at 375 nm

characteristic absorption peak at a wavelength of 375 nm, which is the hallmark optical signature of ZnO NPs arising from the intrinsic band-gap electronic transition specifically, the excitation of electrons from the valence band to the conduction band through photoelectric absorption of UV radiation. The absorption peak recorded at 375 nm represents a slight but meaningful blue shift relative to the absorption edge of bulk ZnO, which typically occurs at approximately 385-390 nm. This blue shift is a direct physical consequence of the quantum size confinement effect: as the particle dimensions approach the nanoscale, the spatial confinement of charge carriers increases the effective bandgap energy of the material, shifting the onset of optical absorption toward shorter wavelengths. The magnitude of the blue shift observed (approximately 10-15 nm from bulk) is in quantitative agreement with the theoretical prediction for ZnO particles in the 20-25 nm size range, providing independent optical corroboration of the particle dimensions established by FESEM analysis. The spectrum further reveals a broad, gradually declining absorption tail extending into the visible and near-infrared regions (400-1000 nm), characteristic of light scattering by the nanoparticle suspension. The absence of any secondary absorption peaks or shoulders confirms that no impurity phases such as zinc hydroxide intermediates or zinc carbonate are present in significant quantities, supporting the phase purity of the synthesized ZnO NP product. The absorption intensity at 375 nm reached a value of approximately 0.78 absorbance units, confirming the successful and reproducible synthesis of ZnO NPs by the chemical precipitation method.

X-ray Diffraction Analysis

X-ray diffraction analysis was performed to confirm the crystalline phase, structural purity, and crystallite size of the synthesized ZnO NPs. The XRD pattern, presented in Fig. 3 and the corresponding peak data summarized in Table 2, revealed a series of well-defined, sharp, and narrow diffraction peaks distributed across the 2θ range of 20°–80°, confirming the high degree of crystallinity achieved following calcination at 500°C for 3 hours. All observed diffraction peaks were successfully indexed to the hexagonal wurtzite

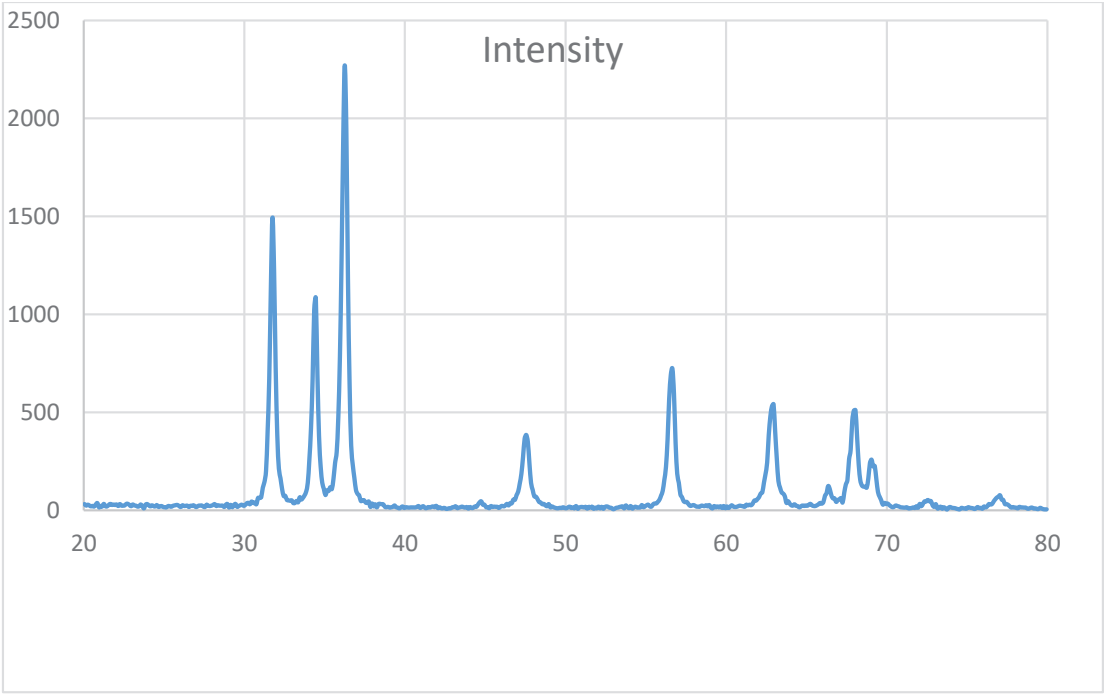

Fig. 3. X-ray diffraction pattern of ZnO NPs synthesized by the chemical precipitation method and calcined at 500°C for 3 hours. most intense peak at 2θ = 36.248° corresponds to the (101) reflection. The absence of secondary phase peaks confirms the phase purity of the synthesized product.

crystal structure of ZnO, in precise agreement with the standard reference diffraction pattern (JCPDS card No. 36-1451).

The most intense diffraction peak in the pattern was recorded at 2θ = 36.248° (d-spacing = 2.478 Å), corresponding to the (101) crystallographic plane of the hexagonal wurtzite ZnO structure, which is the characteristic principal reflection of this phase. Additional prominent peaks observed at 2θ = 31.756° (100), 34.400° (002), 56.603° (103), 62.866° (200), and 67.973° (201) are all characteristic reflections of the wurtzite ZnO phase, in excellent quantitative agreement with the published standard reference pattern. The mean crystallite size of the synthesized ZnO NPs was calculated from by using the Scherrer equation, The Scherrer crystallite size of approximately 22 nm calculated from the XRD data is in excellent agreement with the particle size of 20-25 nm independently determined by FESEM analysis, confirming that each nanoparticle is composed of a single crystalline domain or a very small number of coherently diffracting crystalline domains a characteristic feature of well-annealed, phase-pure ZnO NPs produced by the chemical precipitation method.

Energy Dispersive X-ray Spectrometry (FESEM-EDS) Analysis

FESEM-EDS analysis was employed to simultaneously examine the surface morphology of the synthesized ZnO NPs at high resolution and to confirm their elemental composition with spatial specificity. The EDS spectrum obtained from the synthesized ZnO NP sample is presented in Fig. 4.

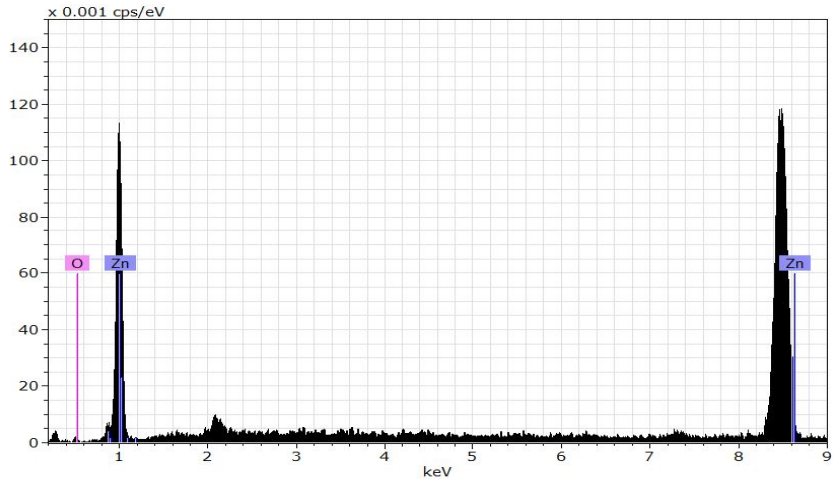

Fig. 4. Energy dispersive X-ray spectrometry (EDS) spectrum of ZnO NPs synthesized by the chemical precipitation method, acquired by field emission scanning electron microscopy (FESEM)

Table 2. XRD peak data for ZnO NPs synthesized by the chemical precipitation method, indexed to the hexagonal wurtzite ZnO phase (JCPDS No. 36-1451).

Peak No.	2θ Position (°)	FWHM (°2Th.)	d-spacing (Å)	Height (cts)	Relative Intensity (%)	hkl Plane
1	31.756	0.3936	2.818	1441.89	66.12	(100)
2	34.400	0.2952	2.607	1015.84	46.59	(002)
3	36.248	0.3936	2.478	2180.59	100.00	(101)
4	44.737	0.3936	2.026	32.13	1.47	(102)
5	47.537	0.3936	1.913	333.56	15.30	(110)
6	56.603	0.4920	1.626	687.50	31.53	(103)
7	62.866	0.3936	1.478	461.30	21.15	(200)
8	66.361	0.2952	1.409	85.16	3.91	(112)
9	67.973	0.3936	1.379	465.50	21.35	(201)
10	69.094	0.4920	1.359	209.66	9.61	(004)
11	72.548	0.4920	1.303	40.39	1.85	(202)
12	76.991	0.4920	1.239	53.04	2.43	(104)

The EDS spectrum reveals the presence of two elements exclusively: oxygen (O) and zinc (Zn), with no detectable peaks corresponding to any extraneous elements, impurities, or contaminants. This binary elemental composition is precisely what is expected for pure zinc oxide (ZnO), and the complete absence of additional elemental signals such as nitrogen (which would indicate residual nitrate from the zinc nitrate hexahydrate precursor), sodium (from the sodium hydroxide precipitating agent), or carbon (from organic contaminants) provides compelling evidence for the chemical purity of the synthesized ZnO NPs. This EDS finding is fully consistent with and complementary to the XRD analysis, which confirmed the hexagonal wurtzite ZnO crystal structure with complete phase purity, and with the UV–visible spectrophotometric analysis, which identified the characteristic ZnO band-gap absorption at 375 nm. Together, the three characterization techniques provide a mutually corroborating, multi-method confirmation of the successful synthesis of chemically pure, crystalline, nanoscale zinc oxide.

Zeta Potential Analysis

The zeta potential of the synthesized ZnO NP suspension was measured to assess the surface charge and colloidal stability of the nanoparticle formulation. The measured zeta potential value of +17.86 Mv as shown in Fig. 5 places the suspension within the transitional zone between incipient instability (±10 to ±20 mV) and moderate stability according to the universally accepted DLVO colloidal stability classification [16]. The positive surface charge is consistent with the protonation of surface Zn-OH groups under the mildly alkaline synthesis conditions employed, producing positively charged Zn-OH_2^+ surface species. While this value falls below the generally accepted threshold of ±30 mV for long-term colloidal stability, it is sufficient to maintain an adequately dispersed suspension for the timescale of experimental preparation and intraperitoneal

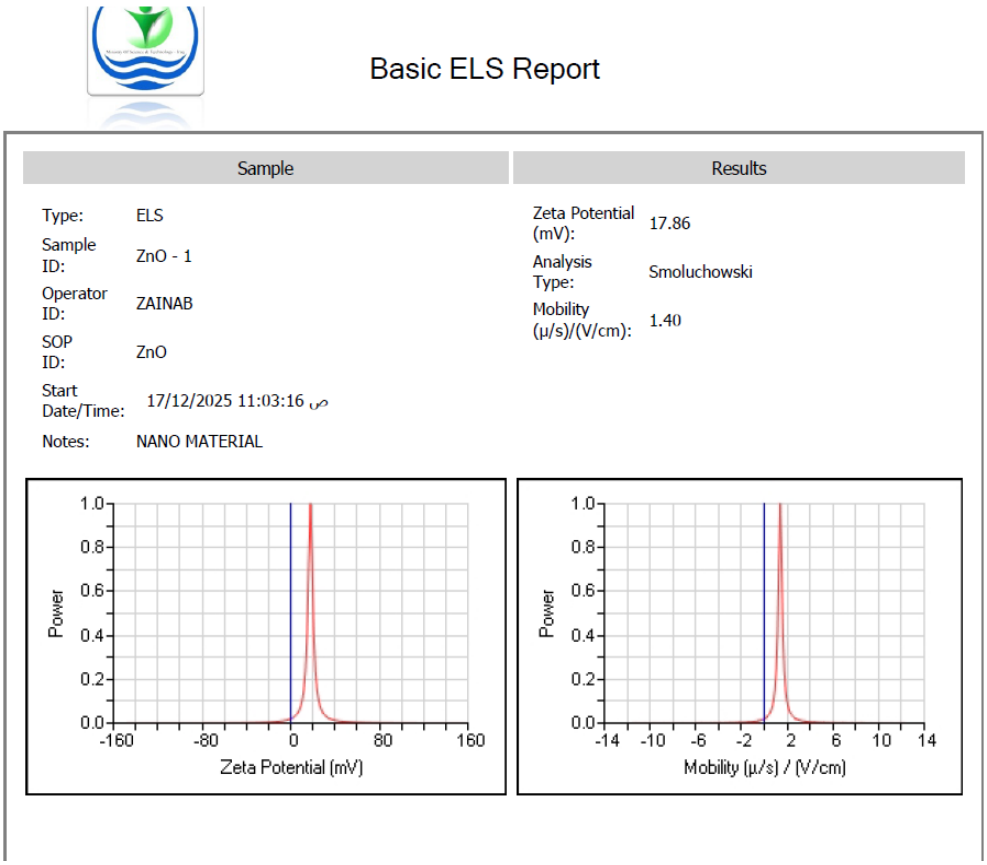

Fig. 5. Zeta Potential Analysis of Synthesized ZnONPs

injection, as confirmed by the absence of visible particle sedimentation during the injection procedure.

Histological and Histomorphometric Effects of ZnO NPs on Hepatic Tissue

Exposure to zinc oxide nanoparticles (ZnO NPs) induced dose-dependent histopathological alterations in the liver tissue of newborn mice. Morphometric analysis revealed a significant reduction in hepatic cell cord thickness in treated groups compared to controls ($p < 0.0001$), indicative of cellular atrophy and parenchymal shrinkage Fig. 6. Histological examination further demonstrated increased hepatocellular death, characterized by nuclear pyknosis, karyorrhexis, and the presence of ghost cellshallmarks of coagulative necrosis particularly in high-dose groups. In animals receiving higher ZnO NP concentrations, marked inflammatory infiltration was observed, comprising lymphocytes, monocytes, and macrophages, accompanied by prominent vascular congestion with erythrocytes accumulation within the hepatic sinusoids. These findings suggest that ZnO NP over exposure triggers both direct cytotoxic effects and secondary inflammatory responses in neonatal liver tissue Fig. 7.

In animals receiving higher ZnO NP concentrations, marked inflammatory infiltration was observed, comprising lymphocytes, monocytes, and macrophages, accompanied by prominent vascular congestion with erythrocyte accumulation within the hepatic sinusoids. These findings suggest that ZnO NP exposure triggers both direct cytotoxic effects and secondary inflammatory responses in neonatal liver tissue.

Immunohistochemical Expression of TNF-α in Hepatic Tissue Following ZnO NP Exposure

Immunohistochemical analysis using anti-TNF-α antibodies revealed a significant, dose-dependent upregulation of TNF-α protein expression in liver tissue ($p < 0.0001$). Quantitative image analysis (AprioScope software) of DAB-stained sections at 40× magnification yielded mean expression values of 14.1 ± 7.6, 151.8 ± 108.3, 427.2 ± 220.8, 1,712.9

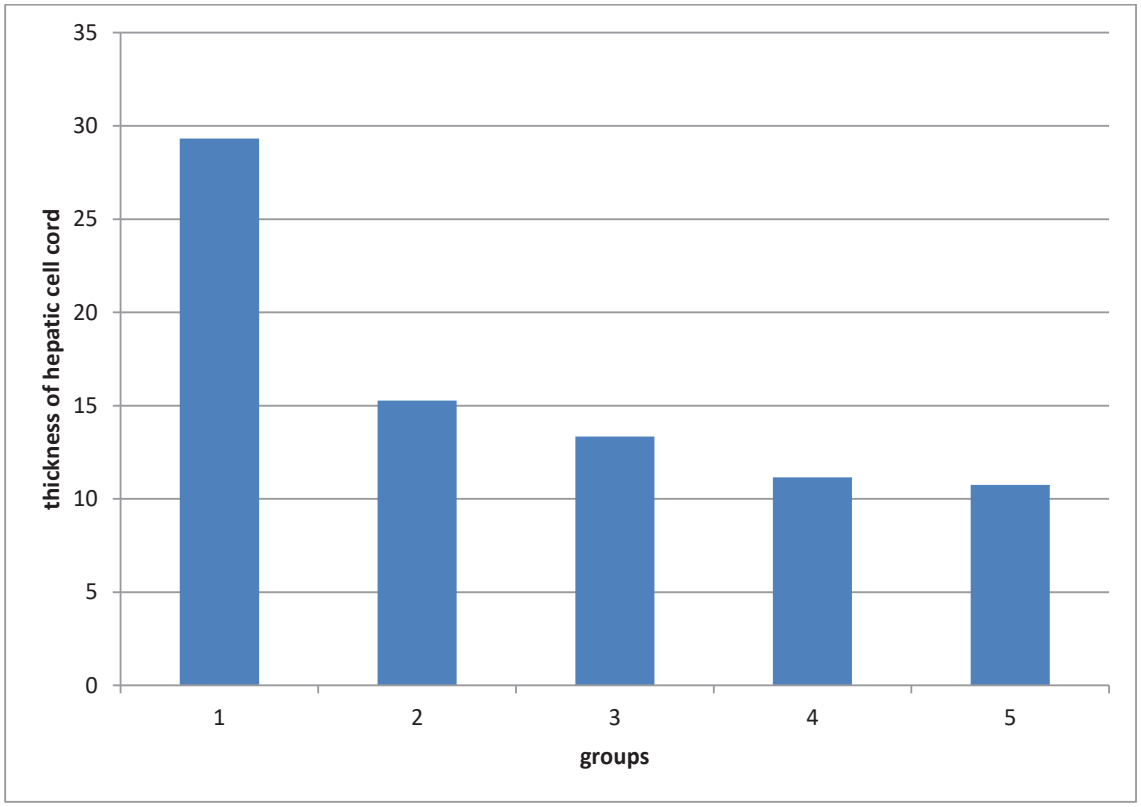

Fig. 6. Bar chart reveals a decrease in thickness of hepatic cells cords (shrinkage) that measured by microns of groups (C, Z0, Z1, Z2, Z3).

± 461.1, and 32,452.8 ± 13,485.8 pixels/µm² for control, Z0, Z1, Z2, and Z3 groups, respectively.

Chemical Precipitation Method: Synthesis and Advantages

The present study successfully employed the chemical precipitation method to synthesize zinc oxide nanoparticles using zinc nitrate hexahydrate [$Zn(NO_3)_2 \cdot 6H_2O$] as the zinc precursor and sodium hydroxide (NaOH) as the alkaline precipitating agent, followed by a two-stage thermal treatment consisting of drying at 100°C and calcination at 500°C. This approach yielded a phase-pure, crystalline ZnO NP product with well-defined

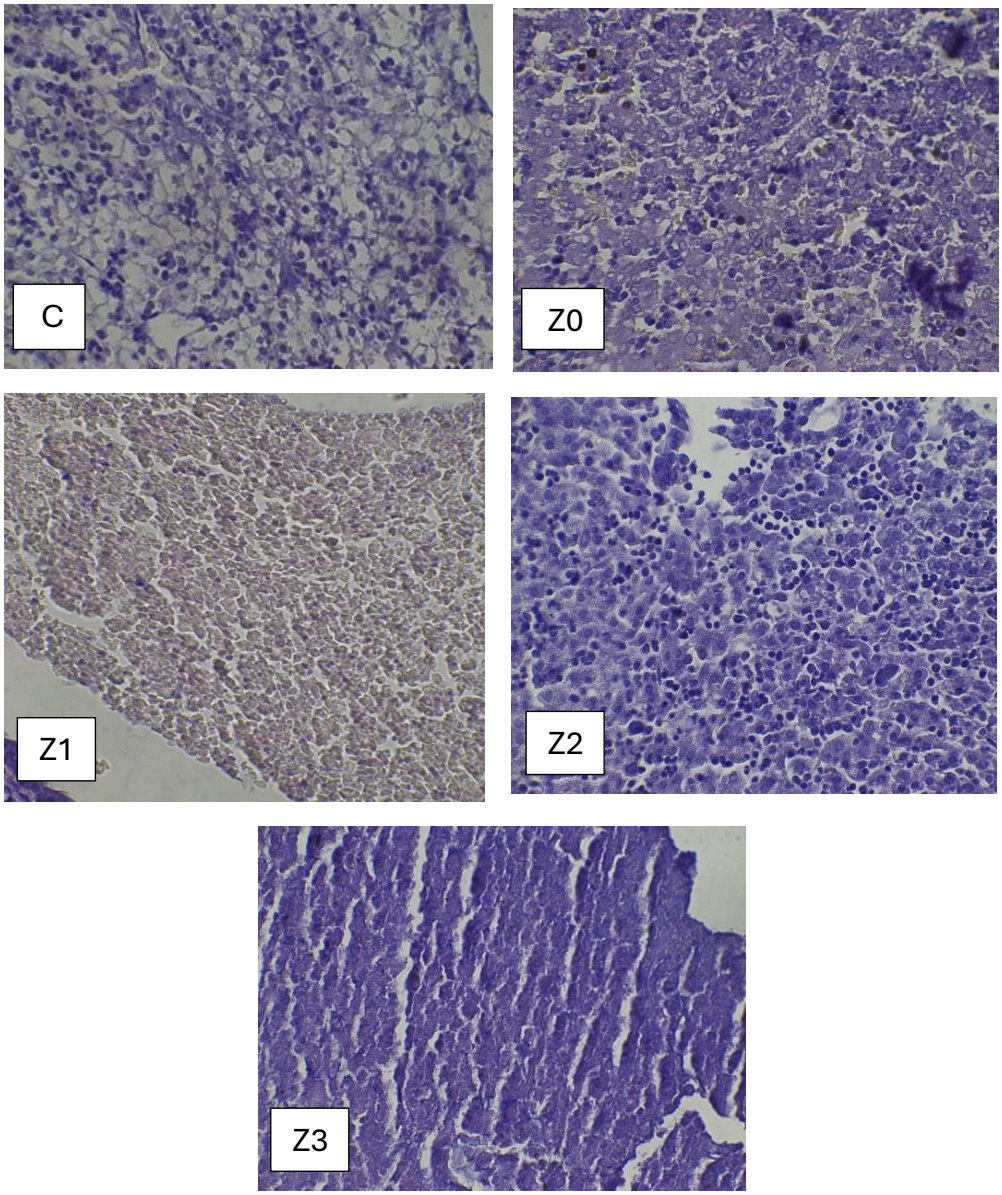

Fig. 7. Reveal decrease in thickness of hepatic cells cords (shrinkage atrophied and thinning) and there were more hepatic cells death of liver tissue with sever liver tissue necrosis that there were absent or ghost and pyknotic nuclei. The high treated groups reveal invasion of various blood cells type (lymphocyte and monocyte cells as macrophage with many red blood cells that mean congested blood vessels with packed RBC in liver parenchyma that were seen in animals treated with Zinc oxide nanoparticles as compare to that of lowest treated and control group at magnification 40X, C for control group, Zo (dose of 5 mg/kg),), Z1(dose of 10 mg/kg), Z2(dose of 20 mg/kg), Z3 (dose of 30 mg/kg).

physicochemical characteristics, confirming the reliability and reproducibility of the chemical precipitation route for the fabrication of ZnO NPs intended for biological evaluation. The chemical precipitation method offers several important practical and scientific advantages that justified its selection in the present study. It requires no specialized equipment, operates under mild conditions (atmospheric pressure, moderate temperatures), and utilizes low-cost, readily available chemical reagents, making it highly accessible and economical for laboratory-scale synthesis [18]. The method affords precise control over particle size and morphology through systematic adjustment of reaction parameters including the molar ratio of zinc precursor to precipitating agent, reaction temperature, stirring speed, and calcination temperature enabling the reproducible production of nanoparticles with defined dimensions across independent synthesis batches [6]. Critically, the calcination step at 500°C for three hours ensured the complete thermal decomposition of the zinc hydroxide intermediate to crystalline ZnO, as confirmed unambiguously by XRD analysis, producing nanoparticles of high crystallinity with consistent and interpretable biological behavior [7].

Characterization of ZnO NPs: Interpretation and Comparison with the Literature

Particle Size, Morphology, and FESEM-EDS

The synthesized ZnO NPs exhibited a mean particle diameter of 20-25 nm with a predominantly spherical morphology, as determined by TEM analysis and corroborated by the Scherrer crystallite size of approximately 22 nm calculated from the XRD (101) reflection. These dimensions fall within the optimal biological size range for nanoparticle-mediated cellular interactions. Nanoparticles in the 10-50 nm range are known to be sufficiently small to undergo cellular endocytosis via clathrin- and caveolae-mediated pathways while being large enough to evade rapid renal clearance, thereby maximizing both cellular internalization efficiency and tissue residence time [19]. The spherical morphology is particularly significant from a toxicological standpoint, as spherical nanoparticles generate greater reactive oxygen species (ROS) per unit mass than anisotropic morphologies such as rods or plates of equivalent volume, owing to their higher surface-area-to-volume ratio and greater proportion of reactive surface sites [20]. The FESEM-EDS analysis provided definitive confirmation of the elemental composition of the synthesized product, revealing exclusively zinc (Zn) and oxygen (O) signals across the full analyzed energy range, with no detectable nitrogen, sodium, or carbon contaminants. This chemical purity is an essential prerequisite for valid in vivo toxicological evaluation, as the presence of ionic contaminants could independently affect cellular function and confound the attribution of biological effects to the ZnO NPs themselves.

UV–Visible Spectrophotometry

The characteristic UV absorption peak at 375 nm recorded in the present study is in excellent agreement with published values for ZnO NPs in the 20–30 nm size range. The slight blue shift relative to the bulk ZnO band edge (~385-390 nm) is a well established physical consequence of quantum size confinement at the nanoscale [21], and the magnitude of this shift is quantitatively consistent with the particle dimensions independently established by FESEM, confirming the reliability of UV-visible spectrophotometry as a rapid, non-destructive method for confirming ZnO NP formation.

XRD Analysis and Crystal Structure

The XRD pattern of the calcined ZnO NPs exhibited twelve characteristic diffraction peaks, all indexed to the hexagonal wurtzite crystal structure (JCPDS No. 36-1451), with the most intense reflection at $2\theta = 36.248°$ corresponding to the (101) plane the principal crystallographic fingerprint of the wurtzite ZnO phase [22]. The complete absence of secondary phase peaks confirms phase purity and the completeness of the thermal decomposition reaction. The calculated Scherrer crystallite size of ~22 nm from the (101) FWHM of 0.3936° is in close agreement with the TEM-determined particle size, confirming single-domain or near-single-domain crystallinity of each nanoparticle. These findings are fully consistent with the XRD characterization of chemically precipitated ZnO NPs reported by Bindu and Thomas [23], who calculated comparable Scherrer sizes from the (101) reflection for similarly prepared samples.

Hepatic Histological Changes in Neonatal Liver: Dose-Dependent Injury

The histological examination of neonatal

liver tissue in the present study revealed a clear, progressive, and dose-dependent pattern of hepatocellular injury following maternal intraperitoneal exposure to ZnO NPs across all treatment groups, with injury severity escalating markedly from the lowest dose (5 mg/kg) through to the most severe changes at the highest dose (30 mg/kg). These findings are highly consistent with and extend the existing body of literature on ZnO NP-mediated hepatotoxicity across multiple animal models and exposure routes. The control group exhibited a fully intact, architecturally normal hepatic parenchyma with regular hepatocyte plates and cords, patent sinusoids, and unremarkable portal tracts, consistent with the classical description of normal hepatic architecture in which hepatocytes are seen arranged in cords radiating from the central vein and separated by normal blood sinusoids [10]. This normal baseline appearance provided a robust comparator against which the dose-dependent injury in treated groups could be reliably assessed. At the lowest dose of 5 mg/kg (Z0), only subtle early histological changes were detectable, including occasional mild congestion and rare nuclear irregularity, with no significant necrosis or extensive inflammatory infiltrate. This is consistent with findings reported by Mansouri et al., who described the infiltration of inflammatory cells with blood congestion, vacuolization of the hepatocyte cytoplasm, and programmed death of certain hepatocytes at low-to-moderate ZnO NP doses [12]. With increasing dose, the histological changes became progressively more severe and widespread. Liver histological analysis in comparable dose-escalation models showed congestion, necrosis, hemorrhage, red blood cell accumulations, and inflammatory cell infiltration with severe abnormalities in high dose groups, while medium and low dose groups showed moderate and least effects, respectively [17]. This dose-dependent pattern of hepatic injury observed in adult Sprague Dawley rats administered ZnO NPs at doses of 10, 20, and 30 mg/kg for 21 days is strikingly parallel to the histological progression documented in the neonatal liver tissue of the present study, despite the fundamental differences in animal age, exposure route, and species, underscoring the consistency and reproducibility of ZnO NP-mediated hepatotoxicity across experimental systems. The thinning and shrinkage of hepatic cell plates and cords documented morphometrically in the present study reflects the loss of hepatocyte volume and structural integrity that accompanies hydropic degeneration and the early stages of necrotic cell death. Hepatocyte vacuolation producing the characteristic foamy or ballooned appearance is widely recognized as a manifestation of intracellular water and lipid accumulation resulting from mitochondrial dysfunction and disruption of membrane ion transport induced by ZnO NP exposure. ZnO NPs have been shown to induce hypertrophy of hepatocytes, nuclear degeneration, focal necrosis, pyknotic nuclei, irregular shaped nucleus and cytoplasmic degeneration in comparable murine models [24], a pattern that closely mirrors the histological findings of the present study, particularly at the intermediate and higher dose levels. The appearance of pyknotic nuclei shrunken, hyperchromatic, condensed nuclei indicating irreversible DNA fragmentation and ghost cells hepatocytes in which all nuclear staining is absent, representing the end stage of necrotic cell death at higher doses in the present study provides histological evidence of progressive and irreversible hepatocellular death. Comparable studies exposing rats to ZnO NPs have demonstrated sinusoidal dilatation, Kupffer cell hyperplasia, lobular and portal triad inflammatory cell infiltration, necrosis, hydropic degeneration, hepatocyte apoptosis, anisokaryosis, and karyolysis [25], findings that closely parallel those documented across the dose range examined in the present neonatal model. The prominent sinusoidal congestion and widespread invasion of the hepatic parenchyma by red blood cells observed at higher doses in the present study is a particularly striking histological finding. This pattern reflects ZnO NP-induced damage to the sinusoidal endothelium the specialized fenestrated endothelial lining of the hepatic sinusoids which disrupts the structural integrity of the sinusoidal wall and allows erythrocytes to extravasate into the perisinusoidal space and the hepatic parenchyma. The compatibility of ZnO NPs with red blood cells at lower concentrations and their increasing aggressiveness toward erythrocytes and endothelial cells at higher concentrations as evidenced by the progressive increase in intraparenchymal RBC invasion with escalating doses in the present study is consistent with the concentration-dependent severity pattern reported by Naz et al. [17]. The dense

infiltration of lymphocytes, monocytes, and macrophages within the hepatic sinusoids and parenchyma at higher doses reflects the activation of innate immune responses to ZnO NP-induced hepatocellular damage. Kupffer cells the resident macrophages lining the hepatic sinusoids and representing the largest population of fixed tissue macrophages in the body are known to become activated upon internalization of ZnO NPs, contributing to amplified local inflammation and tissue destruction [11]. Histological changes in the liver, such as necrosis, destruction of hepatocyte membranes, widening of sinusoidal spaces and vacuolation of their cytoplasm, vascular congestion, and an increased number of Kupffer cells have been similarly documented following ZnO NP administration in mice [12], directly paralleling the inflammatory and structural changes observed in the present neonatal liver model.

Mechanism of ZnO NP-Mediated Hepatocellular Injury

The mechanistic basis for the dose-dependent hepatotoxicity observed in the present study can be understood within a well-established framework of ZnO NP-mediated cellular injury. The principal and most extensively documented mechanism is the intracellular dissolution of ZnO NPs with release of cytotoxic Zn^{2+} ions. Following cellular internalization which occurs primarily through endocytosis in hepatocytes and phagocytosis in Kupffer cells ZnO NPs dissolve within the acidic environment of lysosomes (pH 4.5-5.0), releasing high local concentrations of Zn^{2+} ions into the cytoplasm [26]. Elevated intracellular Zn^{2+} disrupts mitochondrial membrane potential, inhibits the mitochondrial electron transport chain, and triggers the intrinsic apoptotic pathway through cytochrome c release and caspase activation [26]. At sufficiently high intracellular Zn^{2+} concentrations as would be expected at the higher doses tested in the present study the overwhelming of cellular zinc homeostasis mechanisms leads to necrotic rather than apoptotic cell death, producing the ghost cells and confluent necrotic zones observed histologically at the 20 and 30 mg/kg dose levels. This dissolution-driven mechanism is compounded by the direct physical interaction of the positively charged ZnO NP surface (zeta potential +17.86 mV in the present study) with the negatively charged phospholipid bilayer of hepatocyte and sinusoidal endothelial cell membranes, promoting membrane disruption, increased membrane permeability, and facilitated nanoparticle internalization effects that amplify the intracellular delivery of toxic Zn^{2+} ions and contribute to the structural disruption of the sinusoidal endothelium responsible for the red blood cell invasion observed at higher doses [27]. The combination of progressive zinc ion accumulation and membrane-level injury provides a coherent and literature-consistent explanation for the full spectrum of histological changes from mild sinusoidal congestion at low doses to confluent hepatocellular necrosis at the highest dose documented in the present study.

Neonatal Liver Vulnerability and Maternal Transfer

A central and clinically important dimension of the present study is its focus on the neonatal rather than adult liver as the target tissue for toxicological evaluation. The substantially greater severity of ZnO NP-mediated hepatotoxicity observed in the neonatal animals of the present study compared to published data in adult animals at comparable or higher doses reflects the inherently greater vulnerability of the developing fetal and neonatal liver to nanoparticle-induced injury. Oral exposure to ZnO NPs during the period of organogenesis has been shown to significantly enhance maternal-fetal nanoparticle transfer and cause placental dysfunction, leading to fetal developmental toxicity [13]. While the present study employed intraperitoneal rather than oral administration a route that bypasses gastrointestinal absorption and delivers nanoparticles directly to the systemic circulation and peritoneal lymphatic drainage the principle of transplacental nanoparticle transfer applies equally, and the intraperitoneal route would be expected to result in higher systemic bioavailability of ZnO NPs reaching the placental interface than equivalent oral doses [15]. The neonatal liver's particular vulnerability stems from several developmental characteristics: the immaturity of the cytochrome P450 detoxification enzyme system; the high rate of hepatocyte proliferation during the neonatal period, which amplifies genotoxic injury; the ongoing hematopoietic function of the neonatal liver, meaning that hepatocyte loss simultaneously disrupts red blood cell production; and the greater permeability of neonatal cell membranes to ionic species including Zn^{2+} [14]. These factors collectively lower the threshold for nanoparticle-

mediated injury in the neonatal liver relative to the adult organ, explaining the severity of the histological findings reported in the present study at dose levels that produce only moderate effects in adult animals.

Clinical and Regulatory Implications

The findings of the present study carry important implications for the safety evaluation of ZnO NPs in biomedical and consumer product applications, particularly those involving potential exposure during pregnancy. The demonstrated capacity of maternally administered ZnO NPs to produce dose-dependent, severe neonatal hepatotoxicity at doses as low as 5 mg/kg highlights the need for a precautionary approach to ZnO NP exposure in pregnant populations. These findings are also relevant to discussions of the appropriate regulation of ZnO NPs in cosmetic and pharmaceutical products. Regulatory agencies in the United States have determined that zinc oxide is presently recognized as generally safe and effective at concentrations up to 25% for topical use [28], but this regulatory status pertains specifically to dermal application and does not extend to systemic or parenteral exposure scenarios such as those modeled in the present study. While the doses and route of administration employed here are not directly comparable to dermal cosmetic exposure, the mechanistic insights provided particularly the extreme sensitivity of the neonatal liver to ZnO NP-induced injury are scientifically valuable contributions to the broader risk assessment framework for gestational ZnO NP exposure via any systemic route.

CONCLUSION

The present study successfully synthesized phase-pure, crystalline zinc oxide nanoparticles of 20-25 nm diameter and spherical morphology by the chemical precipitation method, with comprehensive multi-method physicochemical characterization TEM, XRD, UV–visible spectrophotometry, FESEM-EDS, and zeta potential analysis confirming the identity, purity, and optical and structural properties of the synthesized product. Maternal intraperitoneal exposure of Swiss albino mice to ZnO NPs at doses of 5, 10, 20, and 30 mg/kg body weight once daily for 18 days produced a clear, dose-dependent pattern of hepatocellular injury in the neonatal liver, characterized by:

Progressive thinning and shrinkage of hepatic cell plates and cords ($p = 0.0001$)

Hepatocyte vacuolation, pyknotic nuclei, ghost cells, and confluent necrosis escalating with dose

Marked sinusoidal congestion, red blood cell invasion of the parenchyma, and dense inflammatory cell infiltration at higher doses

These findings establish that the neonatal liver is a highly sensitive target organ for ZnO NP-mediated developmental hepatotoxicity following maternal exposure. The results highlight the imperative for rigorous safety evaluation of ZnO NPs in reproductive and perinatal contexts and provide a quantitative, multi-parameter toxicological dataset that will inform future dose-response modeling and risk assessment for gestational ZnO NP exposure.

CONFLICT OF INTEREST

The authors declare that there is no conflict of interests regarding the publication of this manuscript.

REFERENCES

1. Nel AE, Mädler L, Velegol D, Xia T, Hoek EMV, Somasundaran P, et al. Understanding biophysicochemical interactions at the nano–bio interface. Nature Materials. 2009;8(7):543-557.
2. Mishra PK, Mishra H, Ekielski A, Talegaonkar S, Vaidya B. Zinc oxide nanoparticles: a promising nanomaterial for biomedical applications. Drug Discovery Today. 2017;22(12):1825-1834.
3. Espitia PJP, Soares NdFF, Coimbra JSdR, de Andrade NJ, Cruz RS, Medeiros EAA. Zinc Oxide Nanoparticles: Synthesis, Antimicrobial Activity and Food Packaging Applications. Food and Bioprocess Technology. 2012;5(5):1447-1464.
4. Jiang J, Pi J, Cai J. The Advancing of Zinc Oxide Nanoparticles for Biomedical Applications. Bioinorg Chem Appl. 2018;2018:1-18.
5. Klingshirn C. ZnO: Material, Physics and Applications. Chemphyschem. 2007;8(6):782-803.
6. Kołodziejczak-Radzimska A, Jesionowski T. Zinc Oxide—From Synthesis to Application: A Review. Materials. 2014;7(4):2833-2881.
7. Kondal N. Effect of high temperature annealing on structural and defect associated properties on ZnO nanoparticles. Materials Today: Proceedings. 2021;37:3056-3057.
8. Sharma V, Anderson D, Dhawan A. Zinc oxide nanoparticles induce oxidative DNA damage and ROS-triggered mitochondria mediated apoptosis in human liver cells (HepG2). Apoptosis. 2012;17(8):852-870.
9. Xia T, Kovochich M, Liong M, Mädler L, Gilbert B, Shi H, et al. Comparison of the Mechanism of Toxicity of Zinc Oxide and Cerium Oxide Nanoparticles Based on Dissolution and Oxidative Stress Properties. ACS Nano. 2008;2(10):2121-2134.
10. Aboulhoda BE, Abdeltawab DA, Rashed LA, Abd Alla MF, Yassa HD. Hepatotoxic Effect of Oral Zinc Oxide Nanoparticles and the Ameliorating Role of Selenium in Rats: A histological,

immunohistochemical and molecular study. Tissue Cell. 2020;67:101441.
11. Watson C, Molina R, Louzada A, Donaghey T, Brain J, Murdaugh K. Effects of zinc oxide nanoparticles on Kupffer cell phagosomal motility, bacterial clearance, and liver function. International Journal of Nanomedicine. 2015:4173.
12. Al-Ragi MJ, Karieb SS, Fathallah N, Zaïri A. Effect of Zinc Oxide Nanoparticles on Liver Functions in Albino Mice. Cureus. 2024.
13. Teng C, Jia J, Wang Z, Sharma VK, Yan B. Size-dependent maternal-fetal transfer and fetal developmental toxicity of ZnO nanoparticles after oral exposures in pregnant mice. Ecotoxicology and Environmental Safety. 2019;182:109439.
14. Sharma V, Singh P, Pandey AK, Dhawan A. Induction of oxidative stress, DNA damage and apoptosis in mouse liver after sub-acute oral exposure to zinc oxide nanoparticles. Mutation Research/Genetic Toxicology and Environmental Mutagenesis. 2012;745(1-2):84-91.
15. Ara C, Andleeb S, Ali S, Majeed B, Iqbal A, Arshad M, et al. Protective potential of fresh orange juice against zinc oxide nanoparticles-induced trans-placental and trans-generational toxicity in mice. Food Science and Nutrition. 2023;11(9):5114-5128.
16. Müller RH, Jacobs C, Kayser O. Nanosuspensions as particulate drug formulations in therapy. Adv Drug Del Rev. 2001;47(1):3-19.
17. Kausar S, Jabeen F, Latif MA, Asad M. Characterization, dose dependent assessment of hepatorenal oxidative stress, hematological parameters and histopathological divulging of the hepatic damages induced by Zinc oxide nanoparticles (ZnO-NPs) in adult male Sprague Dawley rats. Saudi J Biol Sci. 2023;30(9):103745.
18. Wojnarowicz J, Chudoba T, Koltsov I, Gierlotka S, Dworakowska S, Lojkowski W. Size control mechanism of ZnO nanoparticles obtained in microwave solvothermal synthesis. Nanotechnology. 2018;29(6):065601.
19. Rejman J, Oberle V, Zuhorn IS, Hoekstra D. Size-dependent internalization of particles via the pathways of clathrin- and caveolae-mediated endocytosis. Biochemical Journal. 2004;377(1):159-169.
20. Hsiao IL, Huang Y-J. Effects of various physicochemical characteristics on the toxicities of ZnO and TiO2 nanoparticles toward human lung epithelial cells. Sci Total Environ. 2011;409(7):1219-1228.
21. Meulenkamp EA. Synthesis and Growth of ZnO Nanoparticles. The Journal of Physical Chemistry B. 1998;102(29):5566-5572.
22. JCPDS-ICDD Subcommittee Activities. Powder Diffr. 1989;4(1):59-60.
23. Bindu P, Thomas S. Estimation of lattice strain in ZnO nanoparticles: X-ray peak profile analysis. Journal of Theoretical and Applied Physics. 2014;8(4):123-134.
24. Special Issue. Al Hikmah International Journal of Islamic Studies and Human Sciences. 2021;4(Special Issue).
25. Das SK, Sen K, Ghosh B, Ghosh N, Sinha K, Sil PC. Molecular mechanism of nanomaterials induced liver injury: A review. World J Hepatol. 2024;16(4):566-600.
26. Pokhrel S, Xia T, Kovochich M, Liong M, Schowalter M, Rosenauer A, et al. Comparison of the mechanism of toxicity of binary and mixed binary metal oxide nanoparticles based on dissolution and oxidative stress properties. Chem Ing Tech. 2009;81(8):1167-1167.
27. das S, Citra Asmara T, Song Z, Rusydi A, Barbiellini B, Somasundaran P, et al. Probing Biophysicochemical Interactions at Nano-Bio Interface of Perovskite Tandem Biosolar Cells. Biophys J. 2019;116(3):577a.
28. FDA Proposes New Warning For Over-the-Counter Contraceptive Drugs Containing Nonoxynol-9. PsycEXTRA Dataset: American Psychological Association (APA); 2003.